Tectonophysics 510 (2011) 94–103

Contents lists available at ScienceDirect

Tectonophysics

journal homepage: www.elsevier.com/locate/tecto

A study on the influence of the 2008 Wenchuan earthquake on the stability of the Qinghai–Tibet Plateau tectonic block system

Zuan Chen [a,c,*], Banghui Lin [b], Wuming Bai [a], Xu Cheng [a], Yunsheng Wang [c]

[a] Key Laboratory of the Study of Earth's Deep Interior, Institute of Geology and Geophysics, Chinese Academy of Sciences, Beijing 100029, China
[b] Institute of Geophysics, Chinese Seismological Bureau, Beijing 100081, China
[c] State Key Laboratory of Geohazard Prevention and Geoenvironment Protection, Chengdu University of Technology, Chengdu, 610059, China

ARTICLE INFO

Article history:
Received 4 November 2010
Received in revised form 21 June 2011
Accepted 21 June 2011
Available online 1 July 2011

Keywords:
Qinghai–Tibet Plateau
Wenchuan earthquake
Rupture process
Movement and deformation of tectonic blocks
Coulomb failure stress

ABSTRACT

In this paper, the 3D Finite Element Method was combined with a Discontinuous Deformation Analysis (DDA+FEM) to study the influence of the Wenchuan earthquake on the stability of the tectonic blocks system of the Qinghai–Tibet Plateau under the background of northward extrusion of the Indian Plate and obstruction of the strong crust of the Sichuan basin. With constraints from GPS data and focal mechanisms, we first calculated the velocity and stress fields of the region. Then, we numerically simulated the rupture process of the seismogenic fault of the 2008 Wenchuan earthquake in overthrust form with a right-lateral component. We then studied the movement and deformation of the tectonic blocks that was caused by the earthquake and its influence on the stress state of the boundary faults. The numerical simulation indicates that the large earthquake causes the most tectonic blocks in the study zone at approximately a 1-mm deviation toward the northeast; in particular, the Wenchuan seismogenic fault obviously deviated eastwards, and the maximum deviation reaches 1.5 m. It seems that the large earthquake causes the Bayankala block at the west side of the Longmenshan fracture zone to extend farther eastward. The Wenchuan earthquake causes the Coulomb failure stresses on the boundary faults of the tectonic blocks in the study zone to change to different extents. The maximum change of the Coulomb failure stress reaches about 0.2 MPa at both ends of the Wenchuan seismogenic fault, the south section of the Xianshuihe fracture zone and part of the southeast section of the Dongkunlun fracture zone in the upper crust. Additionally, the Coulomb failure stresses also increase to different extents between 0.01 and .02 MPa in regions such as the southernmost end of the Xianshuihe fracture zone, part of the southeast section of the Dongkunlun fracture zone, and so on.

1. Introduction

On May 12, 2008, a destructive earthquake with magnitude of 8.0 occurred on the eastern margin of the Longmenshan fault zone in the Qingzang Plateau. This Ms8.0 earthquake occurred on the boundary fault of the Bayankala Block six and a half years after the 2001 Ms8.1 Kunlunshan earthquake. According to the Chinese earthquake station net, the epicenter of the Wenchuan earthquake was located at 30.95°N,103.40°E. Although there was a slight difference in the source rupture process of the inversion results that were obtained from the seismic wave data of various study groups all over world, these groups do agree that the earthquake occurred on the Longmenshan fracture zone as an overthrust form with a right-lateral component (Chen et al., 2008a; Hua et al., 2009; Liu et al., 2008a; Wang et al., 2008; Zhang et al., 2008). The focal mechanism was close to the overthrust on the southwest section of the seismogenic fault, and the strike-slip component gradually increased, with the rupture extending toward the northeast so that the fault form at the northeast section of the seismogenic fault was mainly a dextral strike slip. The two higher slipping centers along the Longmenshan fault were found from the inversion results of the seismic wave data. Research on the kinetic and dynamic rupture processes of this earthquake under the large background of the Qinghai–Tibet Plateau tectonic block system will have a profound significance in understanding the stability of the tectonic block system of the Qinghai–Tibet Plateau.

Following the Ms7.8 Tangshan earthquake in 1976, China had experienced a decade of seismic quiescence during which no strong earthquake occurred. The active period of Ms≥7.0 strong earthquakes started in 1988; since then, 10 Ms≥7.0 strong earthquakes have occurred, all on the boundary fault of the tectonic blocks of the Qinghai–Tibet Plateau. Since 1996, in particular, strong earthquakes have occurred frequently on the boundary fault around the Bayankala block, including two Ms8.0 earthquakes, four Ms≥7 earthquakes and one nearly Ms7.0 earthquake (see Fig. 1). This trend shows that many locations in the boundary faults of the Qinghai–Tibet Plateau block system, particularly many locations around the Bayankala block, have accumulated sufficient strain energy to approach rupture intensity. It also

* Corresponding author at: Key Laboratory of the Study of Earth's Deep Interior, Institute of Geology and Geophysics, Chinese Academy of Sciences, Beijing 100029, China. Tel.: +86 10 82998421.
E-mail address: zachen@mail.igcas.ac.cn (Z. Chen).

0040-1951/$ – see front matter © 2011 Elsevier B.V. All rights reserved.
doi:10.1016/j.tecto.2011.06.020

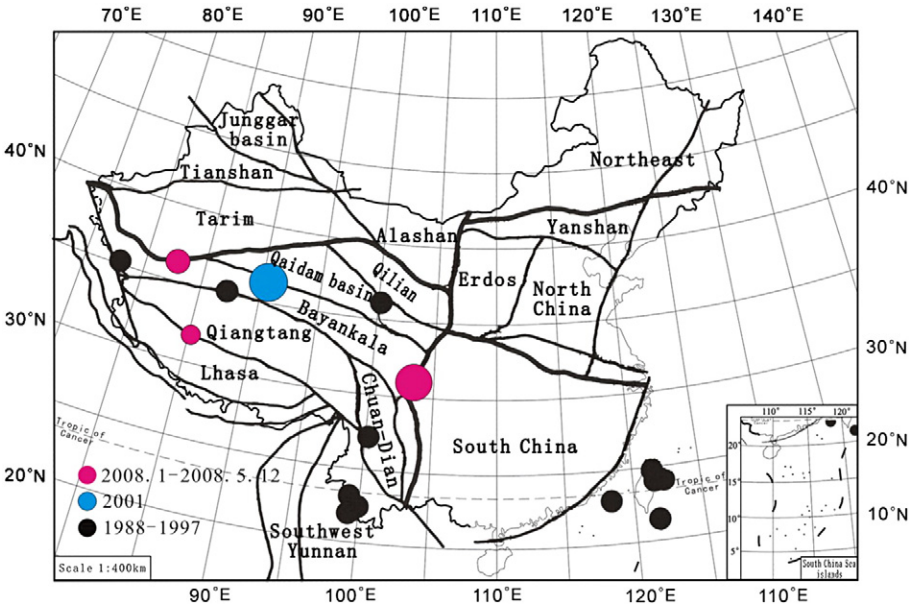

Fig. 1. Distribution map of earthquakes larger than Ms 6.9 and tectonic blocks since 1988.

shows that the strong seismic activities in the Qinghai–Tibet Plateau are more or less related to the deformation and movement of the blocks in the block system. Therefore, research on the influence of the Wenchuan earthquake on the stability of the Qinghai–Tibet Plateau tectonic block system has certain meaning for understanding earthquake risk in the region.

Recently, there have been many studies on the influence of the Coulomb failure stress (CFS) change on the occurrence of subsequent earthquakes. Some important studies were published on this aspect after the Wenchuan earthquake (Parsons et al., 2008; Toda et al., 2008; Wan et al., 2009, 2010). For example, Parsons et al. (2008) calculated CFS changes on faults in the vicinity of the Longmen Shan fault, particularly along the west and northwest rim of the Sichan basin from an elastic dislocation model, and estimated the related earthquake probability. Toda et al. (2008) calculation indicated that the Wenchuan earthquake increase failure stress and seismicity rate on three major fault systems including Xianshuihe, Kunlun and Min Jiang faults, using similar method. Wan et al. (2010) used an updated earthquake source models, updated fault geometric and kinematic parameter to estimate the earthquake potentials in the region.

The purpose of this paper is to attempt a better assessment of CFS changes on boundary faults of the Qinghai–Tibet Plateau tectonic block system using a different method and study path. The study path of this paper is that with constraints from GPS data and focal mechanisms, we first calculated the velocity and stress fields of the region; then, we numerically simulated the rupture process of the seismogenic fault of the 2008 Wenchuan earthquake in overthrust form with a right-lateral component, and finally we study the movement and deformation of the tectonic blocks that were caused by the earthquake and its influence on the stress state of the boundary faults of the tectonic blocks of the Qinghai–Tibet Plateau and its neighboring areas.

2. Brief introduction to DDA + FEM

Our aim is to study stress change on boundary faults of blocks caused by sliding at some section of fault. The critical point lies in how to convert the interactions among all of the blocks into contacts between the blocks. In the end of last century considerable effort has been invested in understanding contact problems with friction (Peric et al., 1992). Numerical method for solving contact problem with friction has been mature. We have developed the 3D DDA + FEM program under some simplifying assumptions, based on previous research works (Chen et al., 2008b; Wang, 2003). DDA is abbreviation of Discontinuous Deformation Analysis which deals with interaction among blocks. FEM is abbreviation of Finite Element Method which deals with deformation inside blocks. In our program, one must suppose that the displacement is very small and that the point of contact among the blocks is known. A brief introduction of DDA + FEM is described as follows.

We assume that the block system consists of many blocks and that each block is divided into some finite elements. The finite elements are hexahedron isoparametric elements. Each element has 8 nodes, with the coordinate of $\mathbf{x}_i$ (i = 1,2…,8), and the displacement of the node is $\mathbf{u}_i$.(i = 1,2…,8). Their shape function is expressed by $N_i(\xi, \eta, \zeta)$ (i = 1,2,…,8), where ξ, η, and ζ are local coordinates.

The displacement model of the finite element is:

$$u = \begin{bmatrix} u \\ v \\ w \end{bmatrix} = [IN_1 IN_2 IN_3 IN_4 IN_5 IN_6 IN_7 IN_8] \begin{bmatrix} u_1 \\ u_2 \\ u_3 \\ u_4 \\ u_5 \\ u_6 \\ u_7 \\ u_8 \end{bmatrix} = Na^e \quad (1)$$

where I is a 3×3 unit matrix.

The relationship between the strain and node displacement of the element is:

$$\varepsilon = [B_1 \quad B_2 \quad B_3 \quad B_4 \quad B_5 \quad B_6 \quad B_7 \quad B_8]a^e = Ba^e \quad (2)$$

where **B** is strain matrix.

The stress of the element is obtained according to the linear elasticity relationship between stress and strain:

$$\sigma = D\varepsilon = DBa^e \quad (3)$$

where **D** is an elasticity matrix containing the appropriate material properties.

Then, the equation of the total functional potential energy based on the minimum potential energy principle is

$$\prod_u = \int_V \frac{1}{2}\varepsilon^T D\varepsilon \, dxdydz - \int_V u^T f \, dxdydz - \int_{S_\sigma} u^T T dS \quad (4)$$

For the discrete model, the potential energy of the system is the sum of the potential energy of all of the elements. That is,

$$\prod_u = \sum_e \prod_u^e = \sum_e \left(a^{eT} \int_{V_e} \frac{1}{2} B^T D B \, dxdydz a^e \right) - \sum_e \left(a^{eT} \int_{V_e} N^T f \, dxdy \right) - \sum_e \left(a^{eT} \int_{S_\sigma^e} N^T T dS \right). \quad (5)$$

We assume that point P on the surface of block A contacts point Q of block B. $\mathbf{x}_P$, $\mathbf{u}_P$, $\mathbf{x}_Q$ and $\mathbf{u}_Q$ are the coordinate and displacement of the contact point. The relationship between the coordinate and displacement of $\mathbf{x}_Q$ and $\mathbf{u}_Q$ and the 8 nodes of the finite element to which point Q belongs are as follows:

$$x_Q = \sum_{i=1}^{8} N_i(\xi_Q, \eta_Q, \varsigma_Q) x_i \quad (6)$$

$$u_Q = \sum_{i=1}^{8} N_i(\xi_Q, \eta_Q, \varsigma_Q) u_i. \quad (7)$$

The displacement of points P and Q on the local coordinate on the contact surface are expressed by u^A and u^B, respectively. When the contact state is bonded, the contact force F^A is expressed by the following formula:

$$F^A = -\lambda \left(u^A - u^B \right) \quad (8)$$

where λ is a virtual spring constant that is generally taken to be so large that penetration between the contact points is prevented. Based on the formula for converting a surface force into an equivalent nodal force, the contribution of n contacts to finite element nodes can be combined into the stiffness matrix of the finite element calculation format.

When the Coulomb criterion is met ($|\tau_s| \geq f \cdot \sigma_n$; τ_s and σ_n are the shearing stress and the normal stress on the contact surface, respectively; f is friction coefficient.), i.e., when it is in the frictional slip contact state, the contact force F^A is expressed as follows:

$$F^A = \begin{bmatrix} \lambda f \left(u_n^A - u_n^B \right) \dfrac{\left(u_x^A - u_x^B \right)}{\bar{u}_T} \\ \lambda f \left(u_n^A - u_n^B \right) \dfrac{\left(u_y^A - u_y^B \right)}{\bar{u}_T} \\ \lambda \left(u_n^A - u_n^B \right) \end{bmatrix} \quad (9)$$

$$\bar{u_x} = u_x^A - u_x^B \quad \bar{u_y} = u_y^A - u_y^B$$
$$\bar{u_T} = \sqrt{\left(u_x^A - u_x^B \right)^2 + \left(u_y^A - u_y^B \right)^2} \quad (10)$$

where f is the friction coefficient. The subscript of the displacement of x and y refers to the displacement that is parallel to the contact surface, and n refers to the normal direction, which is vertical to the contact surface under the local coordinate system.

With regard to contact, we will use the penalty function algorithm to introduce the additional constraint conditions into the function to find the solution. Therefore, the functional is expressed as follows:

$$\prod = \prod_u + \prod_{CP} \quad (11)$$

where $\prod_{CP}$ is the additional functional of the definite solution condition that was introduced using the penalty function. For bonded contact, the functional is:

$$\prod_{CP} = \int_{S_c} \left[\alpha_N \left(u_N^A - u_N^B \right)^2 + \alpha_1 \left(u_x^A - u_x^B \right)^2 + \alpha_2 \left(u_y^A - u_y^B \right)^2 \right] dS \quad (12)$$

For the frictional slip state, the functional is

$$\prod_{CP} = \int_{S_c} \alpha_N \left(u_N^A - u_N^B \right) \left[\left(u_N^A - u_N^B \right) + f(\bar{u}_x / \bar{u}_T) \left(u_x^A - u_x^B \right) + f\left(\bar{u}_y / \bar{u}_T \right) \left(u_y^A - u_y^B \right) \right] dS \quad (13)$$

The equation for the solution of the finite element of the penalty function algorithm is

$$\left({}^tK_L + K_{ca} \right) u = {}^{t+\Delta t}Q - {}^tF \quad (14)$$

where ${}^tK_L$ is the stiffness matrix of the ordinary finite element, K_{ca} is the contribution of the contact surface to the stiffness matrix, ${}^{t+\Delta t}Q_c$ is the additional load caused by the slippage of the contact surface, and ${}^tF$ is the equivalent nodal force of the ordinary additional load.

If lithospheric movement and deformation is considered a long process, assuming that the strain rate is a constant rate within a certain time period, then a similar method to that used for solving elasticity problems can be used for the rheologic dynamic process. Thus, we may obtain initial velocity field and stress field of the study zone by this way. The rheological constitutive relationship is given the following form:

$$\frac{d\varepsilon_c}{dt} = D_c \sigma \quad (15)$$

where ε_c is the rheologic strain tensor and σ the stress tensor, while

$$D_c = \frac{1}{\eta} \begin{bmatrix} 1 & -\mu & -\mu & 0 & 0 & 0 \\ -\mu & 1 & -\mu & 0 & 0 & 0 \\ -\mu & -\mu & 1 & 0 & 0 & 0 \\ 0 & 0 & 0 & 2(1+\mu) & 0 & 0 \\ 0 & 0 & 0 & 0 & 2(1+\mu) & 0 \\ 0 & 0 & 0 & 0 & 0 & 2(1+\mu) \end{bmatrix} \quad (16)$$

where η is the viscosity, and μ is the Poisson ratio.

On simulating numerically the Wenchuan earthquake, we need to solve the nonlinear system of equation shown at Eq. (14) using iterative process and adjusting size of friction coefficient. Because the slip deformation is very small comparing with scale of study zone, the iterative step will pause when the maximum slip displacement and distribution pattern are agreement with the data obtained from the inversion of the seismic wave data and measured in-site by previous research groups. In our trial calculations, we obtained an ideal solution mainly by choosing a group of friction coefficients at different section of seismogenic fault.

3. Block system calculation model and velocity and stress field simulation

In this paper, the Qingzang Plateau, the Sichuan Basin and the eastern side of the Erdos block are selected as the study zone (see Fig. 2a). According to the tectonic block divisions of the Chinese mainland (Zhang, et al., 2003), the study zone was divided into 12 blocks: Tarim, Qaidam, Alashan, Qilian, Bayankala, Qiangtang, Lhasa, Sichuan–Yunnan, Southwest Yunnan, Erdos, the Sichuan Basin and South China. There were nearly 20 block boundary fault zones, including: Altyn, Qilianshan, West Qinling, East Kunlun, West Kunlun, Liupanshan, Helanshan, Mani-Yushu, Kala-Kunlun, Himalayas, Longmenshan, Xianshuihe, Sanjiang, Honghe, Anninghe–Xiaojing, Lancanghe, Qinling–Dabiesha, Fenwei and Yinshan.

The spaces with 120-km vertical depth in the above-mentioned areas are divided into five layers; the region west of the eastern margin of the Qinghai–Tibet Plateau is divided into a 20-km upper crustal layer, a 20-km middle crustal layer, a 30-km lower crustal layer and an upper mantle. Due to the lack of data, with the exception of the Longmenshan fault zone, the boundary faults are all considered

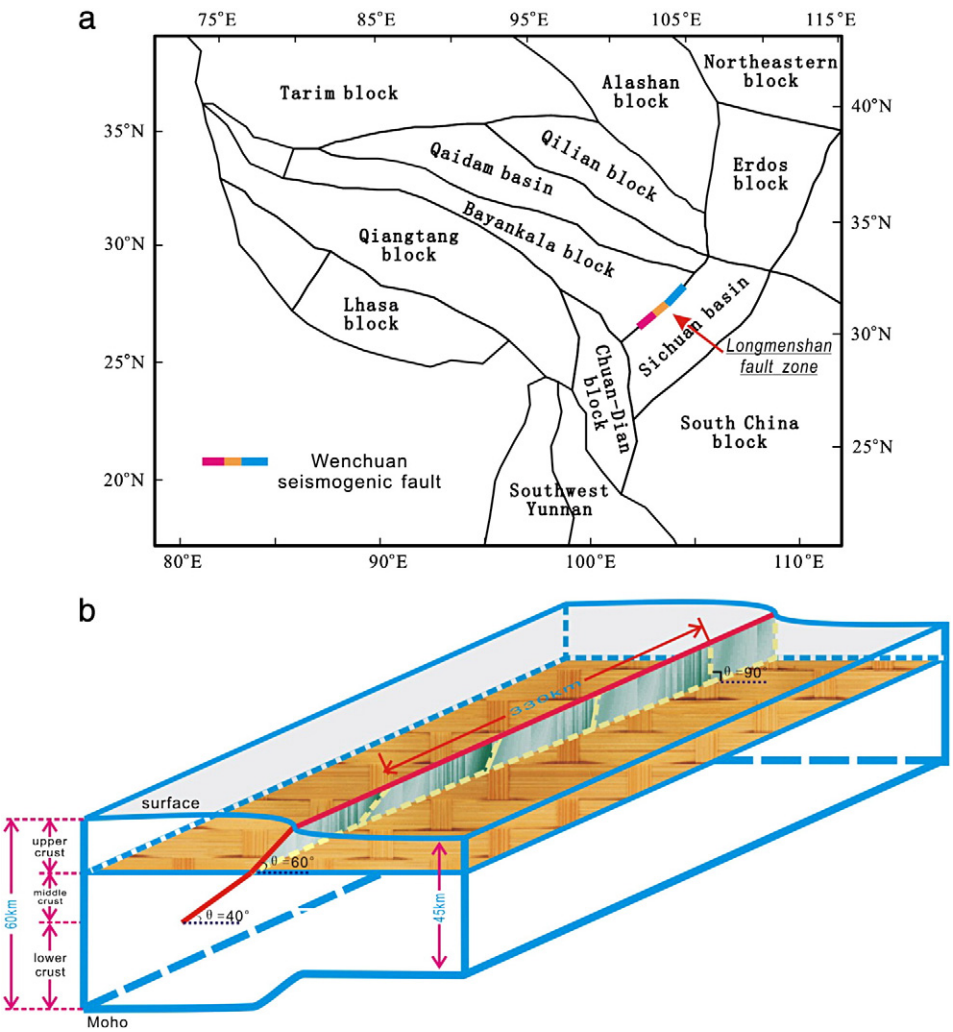

Fig. 2. (a) Tectonic block system model and distribution of seismogenic faults of the Wenchuan earthquake (b) 3D schematic diagram of the seismogenic faults of the Wenchuan earthquake.

Table 1
The mechanical parameters of materials in the model.

Parameters	Region	Young's Modulus (MPa)	Poisson ratio	Density (kg.m^{-3})	Viscosity (Pa.s)	Contact Stiffness (MPa)
Upper crust	(Lhasa block)	550000	0.30	2670	1.7×10^{19}	1.0×10^{10}
	(East Kunlun block: Ganze–Songpan block)	550000	0.30	2670	1.7×10^{19}	1.0×10^{10}
	(Tarim block)	750000	0.30	2680	2.3×10^{19}	1.0×10^{10}
	(Erdos)	800000	0.30	2680	2.52×10^{19}	1.0×10^{10}
	(Sichuan basin)	800000	0.30	2680	2.52×10^{19}	1.0×10^{10}
	(South China block)	700000	0.30	2670	2.2×10^{19}	1.0×10^{10}
	(Northeastern block)	700000	0.30	2670	2.2×10^{19}	1.0×10^{10}
	(Other blocks)	650000	0.30	2700	2.0×10^{19}	1.0×10^{10}
Middle crust	(East Kunlun block: Ganze–Songpan block)	430000	0.25	2780	1.35×10^{19}	1.0×10^{10}
	(Sichuan basin)	930000	0.25	2800	2.93×10^{19}	1.0×10^{10}
	(Erdos block)	850000	0.25	2800	2.68×10^{19}	1.0×10^{10}
	(South China block)	800000	0.25	2790	2.52×10^{19}	1.0×10^{10}
	(Northeastern block)	800000	0.25	2790	2.52×10^{19}	1.0×10^{10}
	(Other blocks)	797000	0.25	2790	2.5×10^{19}	1.0×10^{10}
Lower crust	(Xiangtang block)	450000	0.25	2920	1.4×10^{19}	1.0×10^{10}
	(Sichuan–Yunnan block)	450000	0.25	2920	1.4×10^{19}	1.0×10^{10}
	(East Kunlun block: Ganze–Songpan block)	450000	0.30	2920	1.4×10^{19}	1.0×10^{10}
	(Sichuan basin)	650000	0.30	2940	2.0×10^{19}	1.0×10^{10}
	(Erdos)	650000	0.30	2940	2.0×10^{19}	1.0×10^{10}
	(South China block)	600000	0.30	2930	1.89×10^{19}	1.0×10^{10}
	(Northeast block)	600000	0.30	2930	1.89×10^{19}	1.0×10^{10}
	(Other blocks)	530000	0.30	2930	1.6×10^{19}	1.0×10^{10}
Lithosphere mantle		2120000	0.35	3300	1.0×10^{20}	

to be vertical for simplicity. In the eastern margin of the Qinghai–Tibet Plateau and the areas on the eastern side, the topography on both sides of Longmenshan fault zone and the marked change in the thickness of the crust and its layers are taken into consideration (Burchfiel et al., 2008; Teng et al., 2008; Zhang et al., 2008). The topography rises westwards from an elevation of 500 m in the Sichuan basin to an elevation of 4000 m in the Longmenshan area. The crust in the Sichuan basin is 45 km thick, becomes thicker gradually from east to west and reaches 60 km in the Longmenshan fault zone. The crust of the Qingzang Plateau on the western side is 70 km thick. The upper and middle crust of Longmenshan fault zone is 15 km thick respectively, and the lower crust is 30 km thick. The dip angle in the middle and upper crust of the Longmenshan zone is 40° and 60°, respectively (see Fig. 2b). The initial rupture point of the Wenchuan earthquake is located in the middle crust. To improve the computational accuracy of stress–strain the inside blocks, each block is divided into some finite element grids. The finite element is a hexahedron. The entire block system is divided into 4236 nodes and 3205 units. The bottom is constrained in the vertical direction, and the horizontal direction is moveable. Within a block, the rheological constitutive relationship is used to calculate the velocity field, similarly to the previous work performed by the authors (Chen et al., 2009). In our work, assuming that the strain rate in the lithosphere has a constant rate in a recent time period, then a method similar to that involved in solving elasticity problems can be used for the rheologic process. Within a block, the rheological constitutive relationship (shown as Eq. (15)) is used to calculate the velocity field. On this basis, the stress field and the velocity field are calculated with constraints from GPS data and focal mechanisms. However, the static rock stress that is calculated according to the elastic half space model can be simply added to the initial stress field for the action of gravity. Our model consists of a layered, planar model. The effect on internal stress due to the bending of the plate may be ignored because of the small scale of the study zone in our model.

The P- and S-wave velocity structures vary in the Qinghai–Tibet Plateau and its neighboring areas. Based on the results of the research on the 3D seismic wave velocity structure in the Qinghai–Tibet Plateau (Ding et al., 2001; Liu et al., 2008b; Lou et al., 2008; Teng, 2003; Wang et al., 2003, 2006), different physical parameters are used in this paper for the various crustal layers of the different blocks (see Table 1). The Young's modulus in the upper crust of the Lhasa block which we used in this paper is smaller than in other blocks, but it is relatively greater in the upper crust of the Tarim Basin. Due to high temperature, low velocity, high-conductive layer development and high visco-plasticity of the media in the lower crust, the entire lower crust of the study zone is considered to be a soft layer, especially the lower crust in the Qiangtang block and the Sichuan–Yunnan border block. In the eastern margin of the Qinghai–Tibet Plateau and the areas on its eastern side, the crustal media is considered to be a harder layer in the Sichuan basin and the Erdos block, but it is considered to be relatively low in Sungpan and Ganzi on the western side of the Longmenshan fault zone, especially in the middle and lower crust.

To simulate the rupture process of the Wenchuan earthquake, we must first ensure that the velocity and stress fields in the simulative calculation agree with the velocity field in the Qinghai–Tibet Plateau and its neighboring areas as recorded by GPS data (Zhang et al., 2004) and the stress field in the region as recorded by seismic data (Xu, 2001). In this paper, under the constraints of the GPS results and the focal mechanism solution data, we have obtained the surface velocity field (see Fig. 3a) and the focal mechanism distribution (see Fig. 3b) for some points via simulative calculation under a group of boundary conditions. The simulative focal mechanism is expressed by projecting the main stress acquired via calculation onto a Wulff net. The calculated size of the surface velocity field becomes gradually smaller from the Himalayas fault zone to the Altyn fault zone and the Qilian fault zone. The direction of the velocity changes gradually from NNE in the southwestern Himalayas fault zone to E in the north, and the direction of the displacement in the eastern parts of the Qiangtang block, Kunlun block and the Qaidam block is close to E. The displacement direction changes gradually southward from SE in the western Longmenshan fault zone to SSE in the Sichuan–Yunnan block. The entire image is very similar to the velocity field distribution map acquired from the GPS data. The calculated simulative focal mechanism map shows that the surrounding areas of the Qingzang Plateau have a focal mechanism consisting of thrust faults. The interior of the plateau, especially the Kala-Kunlun fault zone, has a focal mechanism mainly consisting of the stretching of normal faults. However, some parts of the east Kunlun fault zone and the Mani-Yushu fault zone have a focal mechanism consisting of sinistral strike-slip faults, similar to the focal mechanism solution map and the mechanism results for strong earthquakes in recent years that was acquired from seismic wave data. Thus, a foundation was laid for further study.

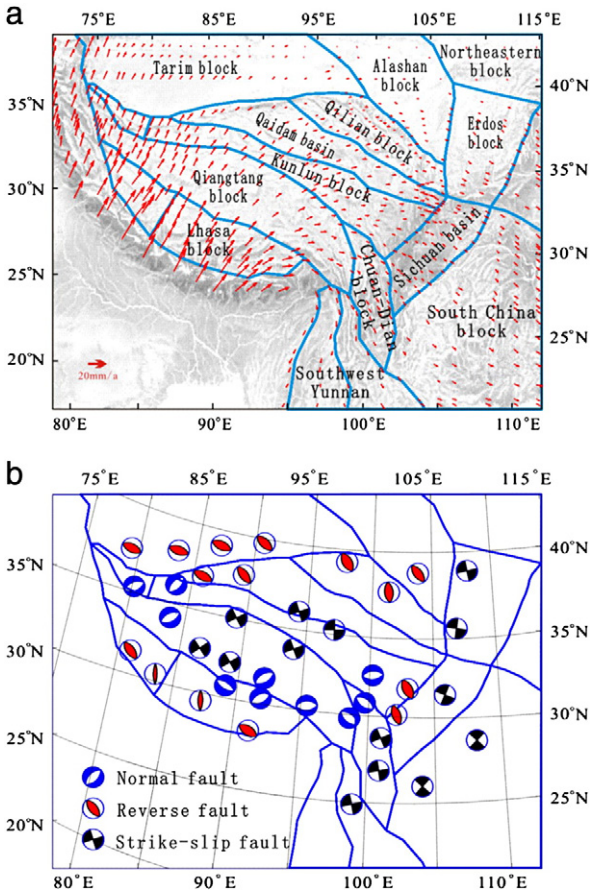

Fig. 3. (a) Distribution of the surface velocity calculated in the study zone. (b) Distribution of the focal mechanism calculated from the stresses tensor in the upper crust of the study zone, using the lower hemisphere stereonet projection.

4. Numerical simulation of the rupture process of the Wenchuan earthquake

Based on the findings of the research that was carried out by Chen et al. (2008a) on the rupture process of this earthquake, this article holds that the seismogenic fault model of the Wenchuan earthquake distributes in upper and middle crust in the Longmenshan fault zone close to the NE strike, which consists of three connected sub-events with southwest to northeast lengths of 100 km, 80 km and 120 km (see Fig. 2a). The dip angles at the southern section of the seismogenic fault are 40° in middle crust and 60° in the upper crust. The middle section is a transform fault; its dip angle gradually increases with northward extension. The dip angle at the northern section of the

seismogenic fault is close to vertical. In this article, the calculated initial velocity and the stress fields basically agree with the velocity field that was acquired from the GPS data and the tectonic stress field from the massive focal mechanism distribution results. Therefore, a perturbation is added onto the initial stress field by reducing the friction coefficient of the seismogenic fault so that the seismogenic fault of the Wenchuan earthquake in the upper and middle crusts becomes unstable, slides according to the Mohr–Coulomb criterion and thus leads to the rupture process of the Wenchuan earthquake.

Fig. 4a is a contour map of the maximum shear stress change before and after the Wenchuan earthquake occurred; it also shows contrast diagrams of the static slide dislocation distribution that was obtained from the inversion of the seismic wave data by three research groups (Chen et al., 2008a; Hua et al., 2009; Wang et al., 2008). The figure shows that there are two center areas with higher shear stress changes on the seismogenic fault of Wenchuan. It also shows that the scale of the high value in the southwest of the fault is larger than that in the northeast of the fault, which basically corresponds to the two higher static slide dislocation areas that were obtained from the inversion of the seismic wave data. Fig. 4b is a contrast diagram of the vertical displacement change vector that was caused by the earthquake and the GPS coseismic vertical displacement of the Wenchuan earthquake that was given by the CEA (CEA, 2009). As shown in the figure, the vertical displacement mainly descends in the east side of the Longmenshan fracture zone, or the Sichuan basin, declining rapidly toward the east, and its maximum value is approximately 1.9 m. However, upward movement is obvious in the northern part of the west side of the fault, the upward scale in middle and south zones is relatively small, and few points for descending in the middle part are found. The overall distribution of the image is similar to the image of the coseismic vertical displacement that was obtained from GPS measurements. Fig. 4c is a contrast diagram of the horizontal displacement change vector that was caused by the earthquake and the GPS coseismic horizontal displacement of the

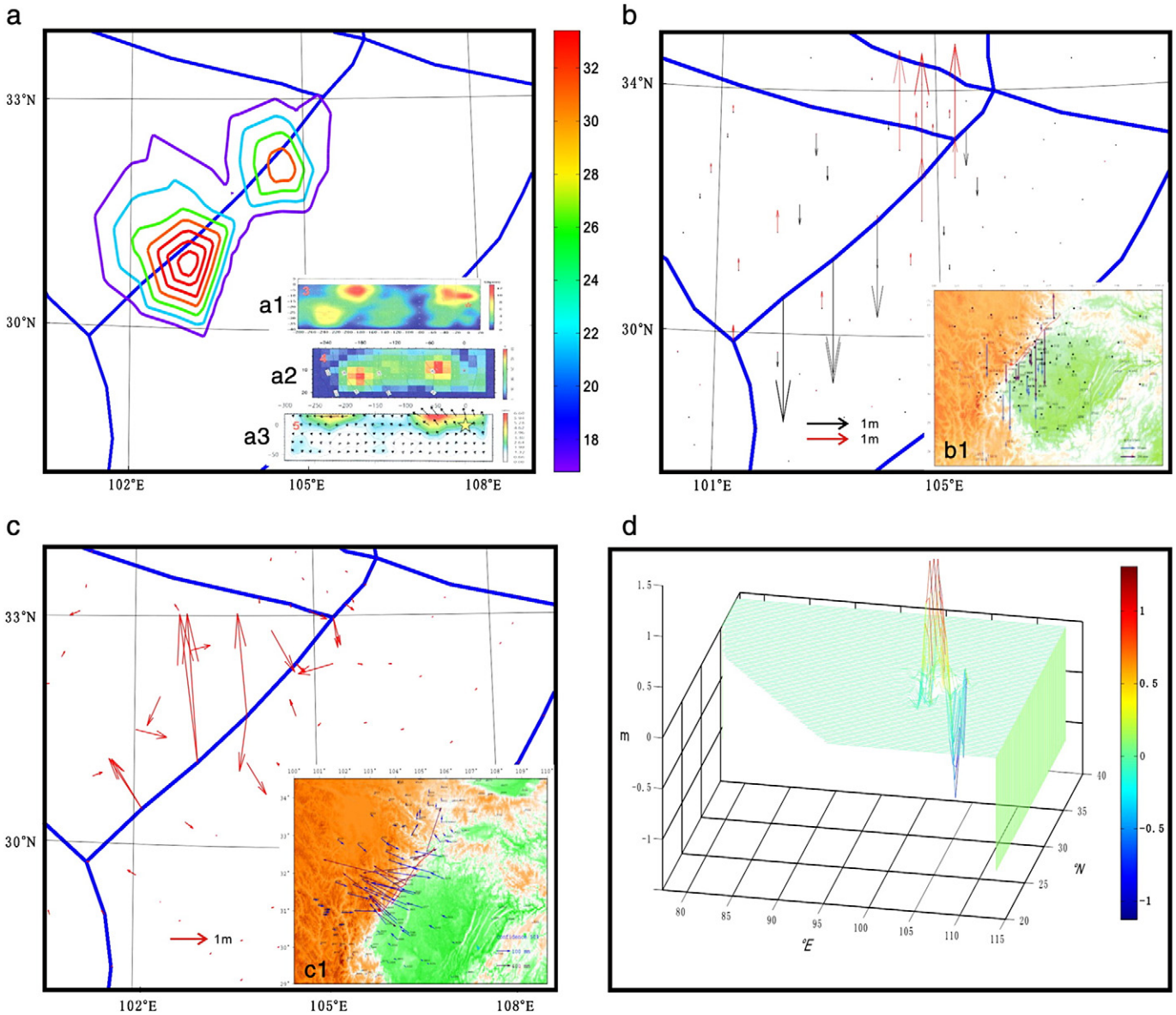

Fig. 4. Contrast diagram of the simulation results of the rupture process of the Wenchuan earthquake. a) Contrast diagram of the maximum stress field change contour and static slide dislocation distribution (a1: Chen et al., 2008a; a2: Hua et al., 2009; a3: Wang et al., 2008). b) Contrast diagram of the vertical displacement change that was caused by the earthquake and the GPS coseismic vertical displacement (b1: CEA, 2009). c) Contrast diagram of the horizontal displacement change that was caused by the earthquake and the GPS coseismic horizontal displacement (c1: CEA, 2009). d) 3D distribution of the vertical displacement that was caused by the earthquake.

Wenchuan earthquake that was given by the CEA (CEA, 2009). As shown in the figure, the calculated horizontal displacement distribution is relatively complex, but overall the pattern shows that the direction of the horizontal displacement in the east side of the Longmenshan fracture zone is mainly northwestward and eastward in the west side of the fault. The scale of the westward horizontal displacement in the east side of the fault is larger than that of the eastward horizontal displacement in the west side of the fault, which results in the sharp shortening of the crust along the horizontal direction. Meanwhile, the decline of the displacement in the east side of the fault is faster than that in the west side of the fault. Fig. 4d is the 3D distribution of the vertical displacement change that is caused by the earthquake, acquired via calculation. As shown in the figure, the displacement on the western side of the Wenchuan seismogenic fault rises and descends on the eastern side of the seismogenic fault, a trend that is agreement with the result obtained from the seismic wave data that the rupture process is of the overthrust type.

The calculated maximum horizontal dislocation of the seismogenic fault in this paper is 5.6 m. The calculated maximum stress drop is 31 MPa which seem to be too high, but it seems to be acceptable considering stronger source rupture of the Wenchuan earthquake. We may give a rough estimate on the stress drop $\Delta\sigma$ as below (Brune, 1970):

$$\Delta\sigma = \frac{7M_0}{16r^3} \tag{17}$$

where M_0 is earthquake moment, r is focal radius. The relationship between earthquake moment M_0 and earthquake magnitude M_L for the Wenchuan earthquake may be obtained through fitting as follows (Hua, et al., 2009):

$$lg\, M_0 = 1.10M_L + 9.31 \tag{18}$$

If we take $M_L = 8.0$, r = 250 km, the stress drop $\Delta\sigma$ is approximately equal to 28 MPa, which is close to our calculated maximum stress drop.

5. The influence of the Wenchuan earthquake on the stress state of the boundary faults of the tectonic blocks of the Qinghai–Tibet plateau and its neighboring areas

On the basis of the numerical simulation on the rupture process of the Wenchuan earthquake, the authors further study the movement and deformation of various tectonic blocks in the study region and the influence of the Coulomb failure stress on the boundary faults that were caused by the Wenchuan earthquake.

Fig. 5 is a map of the movement and deformation of the tectonic blocks after the great earthquake, through enlargement. In the figure, the blue lines represent the boundary of the blocks before the great earthquake, and the red lines indicate the changed boundaries of the blocks that were caused by the great earthquake. As shown in the figure, the Wenchuan seismogenic fault obviously deviates toward the east, and the maximum displacement, about 1.5 m, occurs north of the center of the seismogenic fault. The deviation image indicates that a slide in overthrust form with a right-lateral component occurs in the earthquake, and the Bayankala block in the west side of the seismogenic fault moves farther toward the east. Meanwhile, nearly all of the boundaries of the tectonic blocks in the study region deviate toward the northeast, with a range of about 1 mm. The boundary around the Chuandian rhombus block, especially on the Xianshuihe fracture zone, has a relatively larger change. The numerical simulation result also indicates that the Qinglin-Dabieshan fracture zone at the southern boundary of the Erdos block in the north of China moves and deforms to a relatively larger extent, which seems to implicate that the great earthquake occurrence has some influence on the earthquake risk of the boundary fault of the tectonic blocks in the northeast of China.

To study the influence of the Wenchuan earthquake on the stability of the boundary faults of all of the tectonic blocks, we will calculate the change of the Coulomb failure stress caused by the earthquake on the boundary faults of all of the tectonic blocks. For direct-viewing and easy analysis, we use different colors to express different values of the Coulomb failure stress change. Using Coulomb failure assumption (e.g., Jaeger and Cook, 1969), one can define a Coulomb failure stress CFS such that

$$CFS = \tau_s + f(\sigma_n + p) - S \tag{19}$$

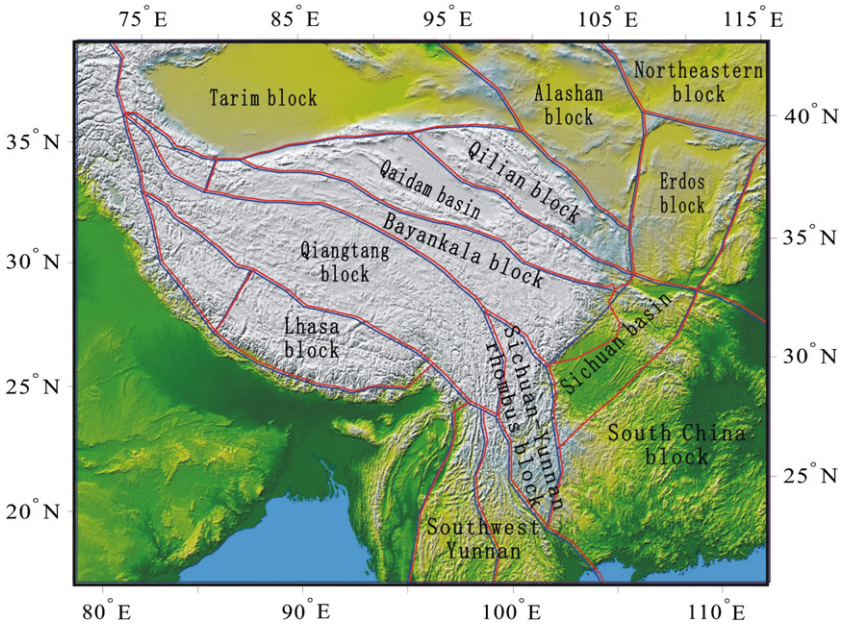

Fig. 5. Map of the movement and deformation of the tectonic blocks after the great earthquake, enlarged (blue lines represent the boundary of the blocks before the great earthquake and the red lines indicate the changed boundary of the blocks that was caused by the great earthquake).

where τ_s refers to the magnitude of the shear stress on the fault plane, σ_n refers to the normal stress (positive for extension) on the fault plane, p is pore pressure, S is the cohesion, and f is the coefficient of friction. If one assumes that f and S are constant over time then a change in CFS is

$$\Delta CFS = \Delta\tau_s + f(\Delta\sigma_n + \Delta p) \tag{20}$$

The $\triangle$ in Eq. (20) indicates the change of parameters. The effect of friction reduction due to pore pressure can be represented by an equivalent friction coefficient $f' = f(1\text{-}B)$, in which B is the Skemton coefficient, in the range of 0–1 (Rice, 1992). Eq. (20) therefore becomes:

$$\Delta CFS = \Delta\tau_s + f'\Delta\sigma_n \tag{21}$$

Where f' is set to 0.4 in this paper. Positive shear stress change $\Delta\tau_s$ and normal stress change $\Delta\sigma_n$ indicate a fault that is close to rupture. Negative $\Delta\tau_s$ and $\Delta\sigma_n$ indicates a fault that is far from rupture. Therefore, the Coulomb failure stress change ΔCFS can express to what degree a fault is close to rupture.

Fig. 6(a, b) shows the distribution of the Coulomb failure stress change that is calculated in the upper and middle crusts of the boundary faults of the Qinghai–Tibet Plateau block system after the Wenchuan earthquake. As shown in the figure, the Coulomb failure stress increase remarkably in some sections, namely near both ends of the seismogenic fault in the upper crust and near the southern and middle sections of the seismogenic fault in middle crust (red areas). Meanwhile, the Coulomb failure stress also increases remarkably in the southern section of the Xianshuihe fault zone and the southeastern section of the Dongkunlunshan fault zone. To compare our result with previous studies, we find that our results are in general agreements with that of Parsons et al. (2008), Toda et al. (2008) and Wan et al. (2010). The change range of the Coulomb failure stress in these zones reaches as high as 0.2 MPa, which is a little larger than their value. The difference is probably resulted from the different calculation methods. In addition, the Coulomb failure stresses in most of the southern end of the Xianshuihe fracture zone, part of the southeast section of the Dongkunlunshan fracture zone, the southwest and southeast edges of the Erdos block, the southeast section of the Xiqinglin fracture zone, part of the southeast section of the Qilanshan fracture zone, and the middle section of the Sanjiang

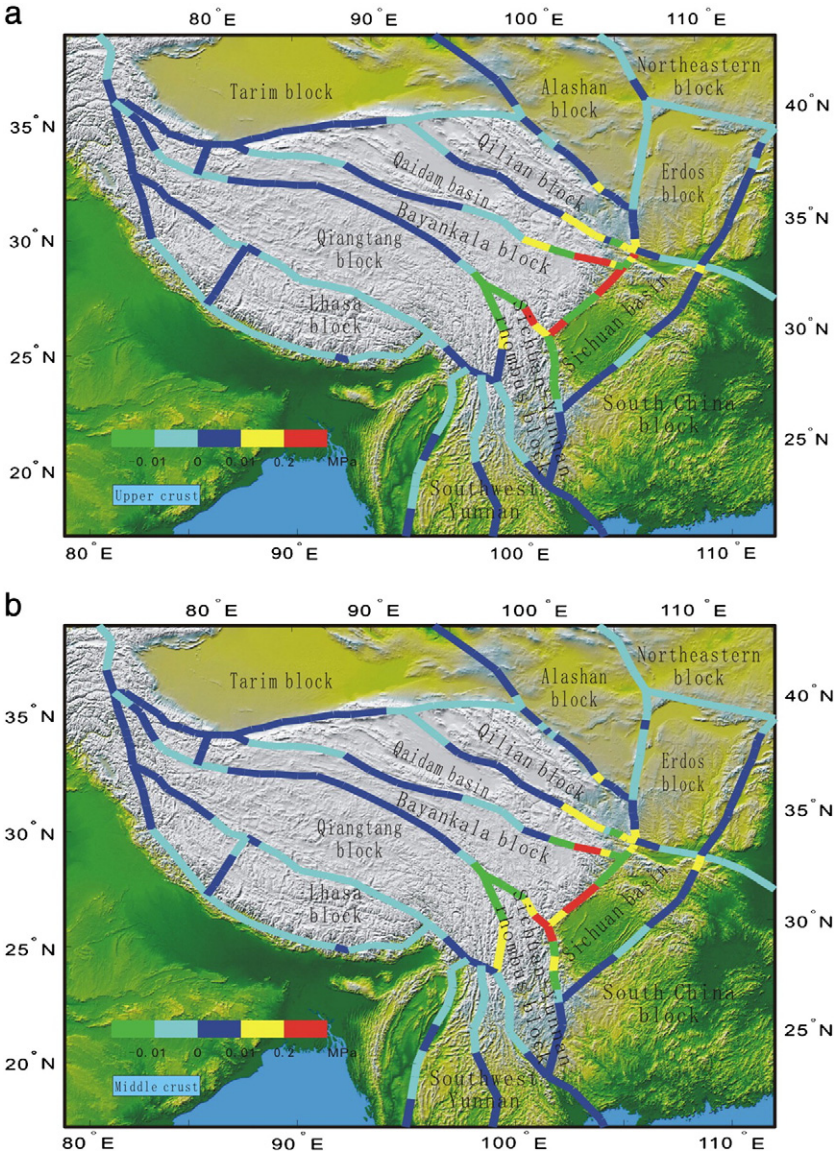

Fig. 6. Distribution of the Coulomb failure stress change on the boundary faults of the Qinghai–Tibet Plateau tectonic block system after the Wenchuan earthquake. (a) upper crust; (b) middle crust.

fracture zone also increase to some extent, ranging from 0.01 to 0.2 MPa.

6. Discussion and conclusion

In this paper, the 3D discontinuous and continuous deformation analysis method is used to numerically simulate the rupture process of the Wenchuan earthquake and to calculate its impact on the stability of the tectonic block systems in the Qinghai–Tibet Plateau under the macro tectonic environment of the strong subduction of several major plates (especially the India Plate) and the inter-constraints that are present among all of the tectonic blocks in the Qinghai–Tibet Plateau and its neighboring areas.

1) The distribution of the surface velocity field in the Qinghai–Tibet Plateau and its neighboring areas that were acquired via calculation essentially agrees with the velocity field result from the GPS data (Zhang, et al., 2004). This calculation offers a base for simulating the rupture process of the Wenchuan earthquake. The simulation of the Wenchuan earthquake in the current work reproduced some of the main features of the earthquake occurrence. This reproduction ensures that the following results obtained in the paper are reasonable.
2) Our results indicate that the Wenchuan earthquake causes Wenchuan seismogenic fault to obviously deviate eastward, and the maximum displacement, about 1.5 m, occurs north of the center of the seismogenic fault. The deviation image indicates that slides of the overthrust form with a right-lateral component occur in the earthquake, and the Bayankala block in the west side of the seismogenic fault moves farther eastward. Meanwhile, nearly all of the boundaries of the tectonic blocks in the study region deviate toward the northeast, with a range of about 1 mm. The boundary around the Chuandian rhombus block, especially on the Xianshuihe fracture zone, has a relatively larger change.
3) The Wenchuan earthquake causes the Coulomb failure stress on various boundary faults of the tectonic blocks in the study region to change to different degrees. The Coulomb failure stress in of the some sections near both ends of the seismogenic fault in the upper crust, the southern section of the Xianshuihe fault zone and the southeastern section of the Dongkunlunshan fault zone increase remarkably, with changes as high as 0.2 MPa. In addition, the Coulomb failure stress in most of the southern end of the

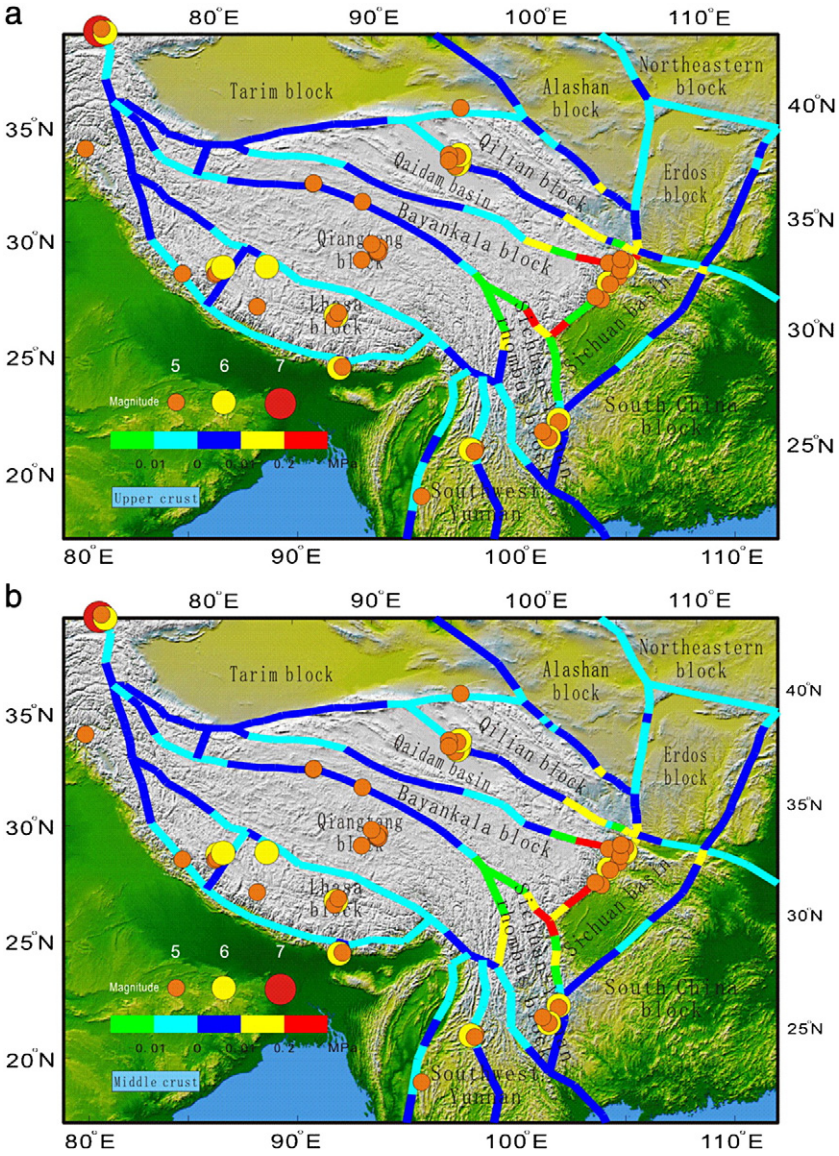

Fig. 7. Distribution map of earthquakes larger than Ms5 that occurred in the study zone from June 1, 2008, to December 31, 2009 (a: upper crust; b: middle crust).

Xianshuihe fracture zone, part of the southeast section of the Dongkunlunshan fracture zone, the southwest and southeast edges of the Erdos block, the southeast section of the Xiqinglin fracture zone, part of the southeast section of the Qilanshan fracture zone, and the middle section of the Sanjiang fracture zone also increase to some extent, ranging from 0.01 to 0.2 MPa. However, any slight increase in the Coulomb failure stress on the highly unstable boundary fault where the accumulated stress is close to the critical state of rupture may possibly lead to the occurrence of a strong earthquake. However, if the accumulated stress on the boundary fault is not close to the critical state of rupture, then the stress change that is caused by the previous earthquake will not trigger the occurrence of the subsequent earthquake. Fig. 7 shows the distribution of larger than Ms5 earthquakes that have occurred in the study zone from June 1, 2008 to December 31, 2009. The majority of the earthquakes that occurred after the Wenchuan earthquake are located in the boundary faults of the tectonic blocks where the Coulomb failure stress increases. The minority of the earthquakes occurred in the boundary faults of the tectonic blocks, where the Coulomb failure stress decreases, or inside the blocks.

4) According to our calculation tests, we find that the results of the calculation that was obtained by the method used in this paper depended on the following factors: (1) the geometrical structure of the tectonic blocks and the boundary faults, (2) the material properties in the 3D model, (3) the boundary conditions, and (4) the friction coefficient. To make the predication closer to reality, we stress that the 3D seismic wave velocity structure, the block dividing result from geology, the GPS data and focal mechanism solutions are very important constraining conditions. It is also important to choose a suitable friction coefficient for the seismogenic fault to simulate the rupture process of an earthquake. The research results for this earthquake must be used as a reference.
5) The mechanical model of the 3D discontinuous and continuous deformation used in this paper is more close to the generation environment of the Qinghai–Tibet Plateau than are other numerical simulation research models. It must be mentioned that the lithospheric structure and the physical properties that were selected in this paper are comparatively simple, especially in the region to the west of the Longmenshan fault zone. With the exception of the seismogenic fault of the Wenchuan earthquake, the boundary faults of the blocks are all vertical. The parameters can only be selected based on the existing seismic wave 3D velocity structures. Such a simplified treatment will have certain influence on the simulation result. We believe that when more data are available in the future, this numerical simulation research will be further improved.

Data and resources

The inversion results about the source rupture process of the Wenchuan earthquake that were obtained from the seismic wave data by Chen et al. (2008a) may be found at http://www.csi.ac.cn/sichuan/chenyuntai.pdf. The location, depth, and magnitude information for the earthquakes occurring from June 1, 2008, to December 31, 2009, came from the China Earthquake Data Center at http://data.earthquake.cn/data/. The analysis software programs used in this article were developed by Chen et al. (2008b).

Acknowledgments

Authors would like to extend my heartiest thanks to Prof. Den Qidong and Dr. Shen Zhengkang for their support and helpful discussions. The authors would also like to thank the editor and two reviewers for helpful discussions and comments. This paper is funded by the program of the National Natural Science Foundation of China (40574017) and the program of the State Key Laboratory of Geohazard Prevention and Geoenvironment Protection (Chengdu University of Technology of China) (DZKJ-0801).

References

Brune, J.N., 1970. Tectonic stress and the spectra of seismic waves from earthquakes. J. Geophys. Res. 75, 4997–5009.
Burchfiel, B.C., Royden, L.H., Van Der Hilst, R.D., Hager, B.H., Chen, Z., King, R.W., Li, C., Lu, J., Yao, H., Kirby, E., 2008. A geological and geophysical context for the Wenchuan earthquake of 12 May 2008, Sichuan, People's Republic of China. GSA Today 18 (7), 4–11.
Chen, Y., Xu, L., Zhang, Y., Du, H., Fen, W., Liu, C., Li, C., 2008a. Report on the Wenchuan larger earthquake source of the May 12, 2008. http://www.csi.ac.cn/sichuan/chenyuntai.pdf.
Chen, Z., Lin, B., Bai, W., 2008b. 3-D numerical simulation on influence of 1997 Mani earthquake to stability of tectonic blocks system in Qingzang and Cuandian regions. Chin. J. Geophys. 51 (5), 1422–1430.
Chen, Z., Lin, B., Bai, W., Cheng, X., Wang, Y., 2009. The mechanism of generation of May 12, 2008 Ms8.0 Wenchuan earthquake. Chin. J. Geophys. 52 (2), 408–417.
Ding, Z., He, Z., Wu, J., Sun, W., 2001. Research on the 3-D seismic velocity structures in Qinghai-Xizang Plateau. Earthquake Res. Chin. 17 (2), 202–209.
Hua, W., Chen, Z., Zhen, S., 2009. A study on segmentation characteristics of aftershock source parameters of Wenchuan *Ms*8.0 earthquake in 2008. Chin. J. Geophys. 52 (2), 365–371.
Jaeger, J.C., Cook, N.G.W., 1969. Fundamentals of Rock Mechanics. Methuen, New York.
Liu, C., Zhang, Y., Xu, L., Chen, Y., 2008a. A new technique for moment tensor inversion with applications to the 2008 Wenchuan Ms 8.0 earthquake sequence. Acta Seismol. Sin. 30 (4), 329–339.
Liu, Q., Chen, J., Li, S., Li, L., Guo, B., Wang, J., Qi, S., 2008b. The Ms 8.0 Wenchan earthquake: preliminary results from the western Sichuan mobile seismic array observations. Seismolog. Geol. 30 (3), 584–596.
Lou, H., Wang, C., Lv, Z., Yao, Z., Dai, S., You, H., 2008. Deep tectonic setting of the 2008 Wenchuan *Ms*8.0 earthquake in southwestern China—Joint analysis of teleseimic P-wave receiver functions and Bouguer gravity anomalies. Sci. China, Ser. D 38 (10), 1207–1220.
Monitor and Predict Bureau, China Earthquake Administration, 2009. Scientific research report on the Wenchuan *Ms*8.0 earthquake. Seismological Press.
Parsons, T., Ji, C., Kirby, E., 2008. Stress changes from the 2008 Wenchuan earthquake and increased hazard in thr Sichuan basin. Nature. doi:10.1038/nature 07177.
Peric, D., Owen, D.R.J., 1992. Computational model for 3-D contact problems with friction based on the penalty method. Int. J. Numer. Mech. Eng. 35, 1289–1309.
Rice, J.R., 1992. Fault stress states, pore pressure distribution, and the weakness of the San Andreas fault. In: Evans, B., Wong, T.F. (Eds.), Fault Mechanics and Transport Properties of Rock. Academic Press, London, pp. 475–503.
Teng, J., 2003. Introduction to Solid Geophysics. Seismological Press.
Teng, J., Bai, D., Yang, H., Yan, Y., Zhang, H., Zhang, Y., Ruan, X., 2008. Deep processs and dynamic responses associated with the Wenchuan Ms8.0 earthquake of 2008. Chin. J. Geophys. 51 (5), 1385–1402.
Toda, S., Lin, J., Meghraoui, M., Stein, R.S., 2008. 12 May 2008 M = 7.9 Wenchuan, China, earthquake calculated to increase failure stress and seismicity rate on three major fault systems. Geophys. Res. Lett. Vol.35, L17305 doi:10.1029.
Wan, Y., Shen, Z., Shen, S., Xu, X., 2009. The influence of 2008 Wenchuan earthquake on surrounding faults. Acta Seismol. Sin. 31 (2), 128–139.
Wan, Y., Shen, Z., Shen, S., 2010. Static Coulomb stress changes on faults caused by the 2008 Mw 7.9 Wenchuan China earthquake. Tectonophysics 491 (4), 105–118.
Wang, C., Wu, J., Lou, H., Zhou, M., Bai, Z., 2003. P-wave crustal velocity structure in western Sichuan and eastern Tibetan region. Sci. China, Ser. D 46 (supp), 254–265.
Wang, C., Wu, J., Lou, H., Chang, L., Su, W., 2006. Study of crustal and upper mantle's structure and mantle deformation field beneath the eastern Tibetan plateau. Earth Sci. Front. 13 (5), 259–349.
Wang, W., Zhao, L., Li, J., Yao, Z., 2008. Rupture process of the Ms 8.0 Wenchuan earthquake of Sichuan, China. Chin. J. Geophys. 51 (5), 1403–1410.
Xu, Z., 2001. A present-day tectonic stress map for eastern asia region. Acta Seismol. Sin. 23 (5), 492–501.
Zhang, P., Deng, Q., Zhang, G., Ma, J., Gan, W., Min, W., Mao, F., Wang, Q., 2003. Active tectonic blocks and strong earthquakes in the continent of China. Sci. China, Ser. D 46 (Supp), 13–24.
Zhang, P., Shen, Z., Wang, M., Gan, W., Burgman, R., Madnar, P., Wang, Q., Niu, Z., Sun, J., Wu, J., Sun, H., You, X., 2004. Continuous deformation of the Tibetan Plateau from global positioning system data. Geology 32, 809–812.
Zhang, P., Xu, X., Wen, X., Ran, Y., 2008. Slip rates and recurrence intervals of the Longmen Shan active fault zone, and tectonic implications for the mechanism of the May 12 Wenchuan earthquake, 2008, Sichuan, China. Chin. J. Geophys. 51 (4), 1066–1073.